Dayside ionosphere of Mars: Empirical model based on data from the MARSIS instrument

F. Němec,[1,2] D. D. Morgan,[1] D. A. Gurnett,[1] F. Duru,[1] and V. Truhlík[3]

Received 8 December 2010; revised 22 April 2011; accepted 28 April 2011; published 13 July 2011.

[1] We present results of a systematic study of electron densities in the dayside Martian ionosphere measured by the Mars Advanced Radar for Subsurface and Ionosphere Sounding (MARSIS) instrument on board the Mars Express spacecraft. There are two distinct regions controlled by different physical mechanisms. The first region is located at altitudes up to about 5 neutral scale heights above the altitude of peak electron density. Electron densities in this region are well described by the basic Chapman theory. The observed small deviations can be most probably explained by the neutral scale height and electron temperature increasing with altitude rather than being constant. The second region is located at altitudes higher than about 10 neutral scale heights above the altitude of peak electron density. It is controlled primarily by diffusion, and the observed electron densities decrease exponentially with increasing altitude. The corresponding diffusion scale height increases with increasing solar zenith angle, which can be probably explained by nearly horizontal magnetic fields in the ionosphere induced by interaction with the solar wind. The obtained dependencies can be used as a simple empirical model of the dayside Martian ionosphere.

Citation: Němec, F., D. D. Morgan, D. A. Gurnett, F. Duru, and V. Truhlík (2011), Dayside ionosphere of Mars: Empirical model based on data from the MARSIS instrument, *J. Geophys. Res.*, *116*, E07003, doi:10.1029/2010JE003789.

1. Introduction

[2] The classical Chapman theory [*Chapman*, 1931a, 1931b] turns out to be a relatively good description of the dayside ionosphere of Mars at altitudes near the altitude of the ionospheric peak [*Gurnett et al.*, 2005, 2008; *Morgan et al.*, 2008; *Withers*, 2009]. This theory takes into account only photoionization and recombination, neglecting, among other things, any plasma transport. Moreover, it assumes a single ionizing photon energy and the neutral scale height H and reaction coefficients to be constant over all the altitudinal range. According to this theory, the electron density n at any given altitude z is equal to

$$n(z) = n_m \exp\left\{\frac{1}{2}\left[1 - \frac{z - z_m}{H} - \exp\left(-\frac{z - z_m}{H}\right)\right]\right\} \quad (1)$$

where n_m is the peak electron density and z_m is the altitude of peak electron density.

[3] Concerning the solar zenith angle (SZA) dependence of the used parameters, the Chapman theory predicts that the peak electron density decreases with increasing SZA as

$$n_m = \frac{n_0}{\sqrt{Ch}} \quad (2)$$

where n_0 is the peak electron density at the subsolar point and Ch is the so-called Chapman grazing incidence function that takes into account the absorption of solar radiation as it passes obliquely through the ionosphere. For not very large SZAs the Chapman grazing incidence function can be reasonably well approximated by 1/cos(SZA). At Mars, the cosine approximation breaks down beyond around 75° (see *Smith and Smith* [1972, Figure 7] for SZA dependence of its deviation from real values, with $X_{Mars} = (z + R_{Mars})/H \approx 300$). The altitude of peak electron density is predicted to increase with increasing SZA as

$$z_m = z_0 + H \ln Ch \quad (3)$$

[4] At higher altitudes transport processes start to play an important role and eventually control the structure of the dayside ionosphere [*Chen et al.*, 1978; *Rohrbaugh et al.*, 1979; *Fox and Dalgarno*, 1979; *Withers*, 2009]. The deviations of the ionospheric profiles measured by the Mars Advanced Radar for Subsurface and Ionospheric Sounding (MARSIS) on board the Mars Express spacecraft [*Chicarro et al.*, 2004] toward electron densities larger than the ones expected according to the Chapman theory represent an indication of such a transition [*Gurnett et al.*, 2008; *Duru et al.*, 2008]. *Duru et al.* [2008] used local electron density data from the MARSIS instrument to analyze median electron density profiles in the altitude range from about 300 to 1200 km as a function of SZA. These authors have shown that the electron density decreases exponentially with increasing altitude. The appropriate scale height was found to increase considerably with increasing SZA, from about 80 km near the subsolar point up to 145 km close to the

[1]Department of Physics and Astronomy, University of Iowa, Iowa City, Iowa, USA.
[2]Now at Institute of Atmospheric Physics, Academy of Sciences of the Czech Republic, Prague, Czech Republic.
[3]Institute of Atmospheric Physics, Academy of Sciences of the Czech Republic, Prague, Czech Republic.

0148-0227/11/2010JE003789

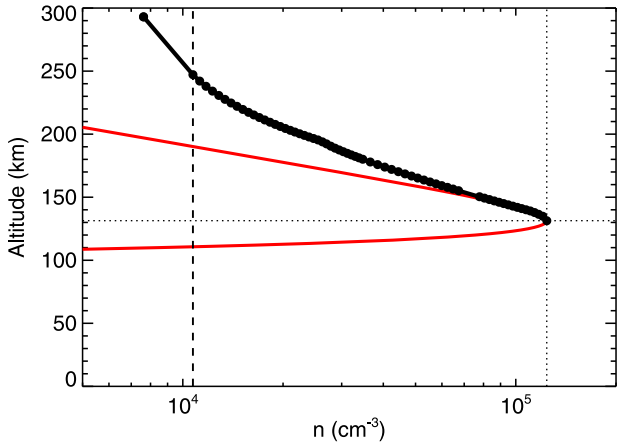

Figure 1. An example of one of the analyzed ionospheric profiles. The measured data are shown by solid black circles. The solid black curve represents an exponential interpolation. The vertical dashed line marks the lower detection limit of the sounding instrument for this particular event. A single data point of lower electron density was obtained by the analysis of local electron plasma oscillations. Peak electron density and altitude of peak electron density are marked by dotted lines. The best fit Chapman electron density profile is shown by the red curve.

terminator. The role of the crustal magnetic fields of Mars on the observed electron density variations was discussed by *Duru et al.* [2008], who concluded that at the high altitudes included in the study crustal fields are expected to have little influence. However, the role of the magnetic field induced in the ionosphere due to the interaction with the solar wind [*Crider et al.*, 2001; *Brain et al.*, 2003; *Crider et al.*, 2004] was not discussed. This induced magnetic field is known to be strongest and nearly horizontal at the subsolar point, with the magnetic field inclination increasing as a function of SZA [*Brain et al.*, 2003; *Crider et al.*, 2004].

[5] In the present study we report the overall results obtained for the dayside ionosphere of Mars using the data from the MARSIS instrument onboard the Mars Express spacecraft. Ionospheric profiles obtained by the topside ionospheric sounding and local measurements of electron density are combined to obtain the best possible data coverage. The two regions of the dayside ionosphere are identified and simple relations describing the electron densities are derived, resulting in an empirical model of electron density in the dayside ionosphere of Mars.

[6] The electron density data acquired by the MARSIS instrument since August, 2005 till the end of 2009 have been used. MARSIS is a topside ionospheric sounder on board the Mars Express spacecraft (eccentric orbit around Mars, periapsis altitude 275 km, apoapsis altitude 11,000 km, orbital inclination 86°, orbital period 6.75 h; see *Chicarro et al.* [2004] for more details). A more detailed description of the MARSIS instrument is given by *Picardi et al.* [2004] and *Jordan et al.* [2009]. The connected data processing is described by *Gurnett et al.* [2005], *Duru et al.* [2008], and *Morgan et al.* [2008].

[7] The existence of the two regions of the ionosphere is demonstrated in section 2. These are separately discussed in sections 3 and 4. Section 5 gives an empirical guide to estimation of electron densities in the transition region between the two regions. A brief overview of the key functions and parameters that form the empirical model is given in section 6. Our results are discussed in section 7. Section 8 contains a brief summary of the main results.

2. Two Regions of the Dayside Ionosphere

[8] Altogether, we have analyzed 30,283 density profiles acquired at SZAs less than 100°. Since the sounding frequencies are logarithmically spaced with $\Delta f/f \approx 2\%$ [*Duru et al.*, 2008], the electron plasma frequency can be measured with an accuracy of about ±1%. This corresponds to an accuracy for measuring the electron density of about ±2%. The uncertainty for measuring the apparent range is about ±6.8 km [*Morgan et al.*, 2008]. The uncertainty of the corrected range is difficult to determine, but it is expected to be roughly the same. For each of the density profiles we have determined the best fit Chapman model (see section 1), yielding the following three Chapman parameters: peak electron density n_m, altitude of the peak electron density z_m, and neutral scale height H. An example of one of the analyzed profiles is shown in Figure 1. The electron densities determined as a function of altitude are plotted as solid black circles. The solid black curve represents an exponential interpolation. The vertical dashed line represents the lower detection limit of the MARSIS sounding measurement for this particular event. A single data point determined from local plasma oscillations was used to determine the plasma density at the spacecraft [*Duru et al.*, 2008]. The best fit Chapman model is given by a solid red curve. The peak electron density and the altitude of peak electron density are marked by vertical and horizontal dotted lines, respectively. In addition to the ionospheric profiles obtained by ionospheric sounding, nearly 200,000 local measurements of electron density obtained by the analysis of local electron plasma oscillations at SZA < 100° were included in the study.

[9] It can be seen that the Chapman profile shown in Figure 1 gives a good fit to the observed electron densities close to the altitude of peak electron density in the ionosphere. However, at higher altitudes there are significant differences. These deviations turn out to be rather systematic, with observed electron densities being generally larger than the ones predicted by the Chapman theory [*Gurnett et al.*, 2005, 2008]. A transition between the photoequilibrium-dominated region at low altitudes and the transport-dominated region at high altitudes [*Chen et al.*, 1978; *Rohrbaugh et al.*, 1979; *Fox and Dalgarno*, 1979] has been suggested as a possible explanation. Additionally, the electron temperature T_e significantly increases at these altitudes [*Hanson and Mantas*, 1988], which slows down the recombination rates [*Schunk and Nagy*, 2000] (see *Lillis et al.* [2009, Figure 2d] for an altitudinal dependence of the recombination rate.

[10] In order to study the observed electron densities as a function of altitude in a more systematic way, we have organized all the measured data as a function of the two crucial parameters used in the Chapman theory: (1) the ratio of electron density and peak electron density (n/n_m) and (2) the altitude relative to the altitude of peak electron density normalized by the neutral scale height ($(z - z_m)/H$). The

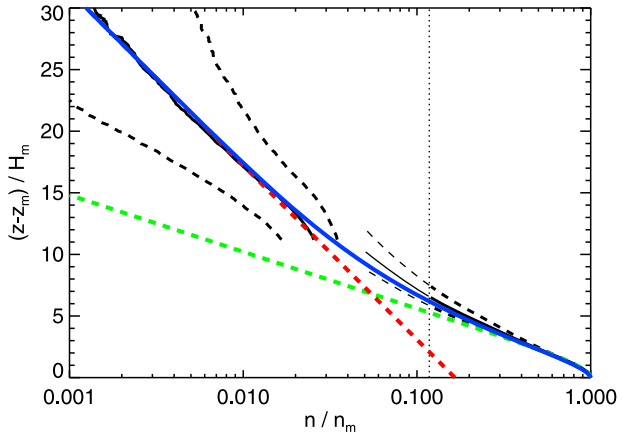

Figure 2. Observed electron densities normalized by peak electron densities organized as a function of altitude relative to the altitude of peak electron density normalized by the neutral scale height. The vertical dotted line marks the median lower detection limit of ionospheric sounding. The solid black curves represent median values of observed electron densities. The dashed black curves represent 0.25 and 0.75 quartiles. The Chapman profile, expressing the dependence observed at altitudes near the ionospheric peak, is shown by the dashed green curve. An exponential decrease of electron density with altitude, expressing the dependence observed at higher altitudes, is shown by the dashed red line. The blue curve traces the empirical fit connecting smoothly the two regions (see section 5).

results are shown in Figure 2. A vertical dotted line marks the median detection limit of the ionospheric sounding.

[11] Data to the right of this line (i.e., at larger electron densities) were obtained primarily by ionospheric sounding. However, in some cases the electron densities were lower than the detection threshold of ionospheric sounding. In such cases, the electron density was estimated using an exponential interpolation between the lowest-density data point obtained from ionospheric sounding and a data point obtained by the local electron density measurement. The median value of electron densities is plotted by a solid black curve, and 0.25 and 0.75 quartiles are plotted by dashed black curves in Figure 2.

[12] Electron densities lower than the median detection limit usually cannot be detected by ionospheric sounding. However, they are often still large enough to be determined by a significantly more sensitive analysis of local electron plasma oscillations. The corresponding values of median and 0.25/0.75 quartile electron density are shown in the high-altitude low-density part of Figure 2 using the same representation as described above for the sounding results. Moreover, the electron densities at altitudes between the satellite altitude and the altitude where the electron density reaches the ionospheric sounding detection limit can be estimated by using an exponential interpolation. These data points can be used to extend the range of data obtained by ionospheric sounding to slightly lower densities. However, as lower densities are approached and the ratio of data obtained solely from exponential interpolation increases, the precision of such an approach decreases significantly. Thus, we have limited this type of analysis to an arbitrarily chosen threshold of $n/n_m > 0.05$. The corresponding median value is shown by a thin solid black curve and the appropriate 0.25 and 0.75 quartiles are shown by thin dashed black curves.

[13] The dashed green and red curves show two simple analytical approximations of the observed dependence. The green curve is a dependence corresponding to the Chapman profile according to equation (1). The red curve represents an exponential decrease of electron density with increasing altitude and is used to express the dependence observed in the high-altitude region. The solid blue curve shows the result of an empirical model that is described in section 5 and that smoothly connects the two extreme dependencies.

[14] Two different regions can be clearly identified. Electron densities at altitudes up to about 5 neutral scale heights above the altitude of peak electron density are well described by the Chapman-predicted profile. Hereinafter, this region will be referred to as the "Chapman" region. Electron densities at altitudes larger than about 10 neutral scale heights above the altitude of peak electron density decrease exponentially with increasing altitude, corresponding to diffusion-like behavior. This region will be referred to as the "diffusion region". Between these two regions, at altitudes from about 5 to 10 neutral scale heights above the altitude of peak electron density, there is a "transition region" where the resulting dependence is a combination of the two extremes.

[15] The reason why these two regions are formed and our choice of this terminology become clear when one considers that the Chapman theory includes photochemical processes but neglects plasma transport. Close to the altitude of peak electron density, where the timescales of plasma transport processes τ_D are much longer than the photochemical timescales τ_{PC}, such an approximation is sufficient. However, since τ_{PC} increases exponentially with altitude and τ_D decreases exponentially with altitude, transport processes at larger altitudes become more important and eventually control the structure of the dayside ionosphere [see *Withers*, 2009, and references therein]. This corresponds exactly to the dependence observed in the MARSIS data.

[16] Note that although *Duru et al.* [2008] reported ionopause detections in MARSIS data, there is no hint of an ionopause in Figure 2. This is probably due to the fact that an ionopause appears to be absent greater than 80% of the time [*Duru et al.*, 2008]. As such a rare phenomenon it does not affect the average results. Hereinafter, we are neglecting the possibility of an ionopause in our study.

3. Chapman Region

[17] As we show in section 2, electron densities in the Chapman region of the dayside ionosphere of Mars can be described by the basic Chapman theory expressed by equation (1). It is thus of great importance to know the three "free" parameters, n_m, z_m, H, needed to evaluate this equation at any given altitude z.

[18] In the basic Chapman theory the neutral scale height H is supposed to be constant over all altitudes and SZAs. The values n_m and z_m can be calculated from the values n_0 and z_0 at the subsolar point using equations (2) and (3), respectively. However, this does not entirely correspond to the dependence observed in the MARSIS data, most likely because both the neutral scale height H and electron temperature T_e increase with increasing altitude. A variation of

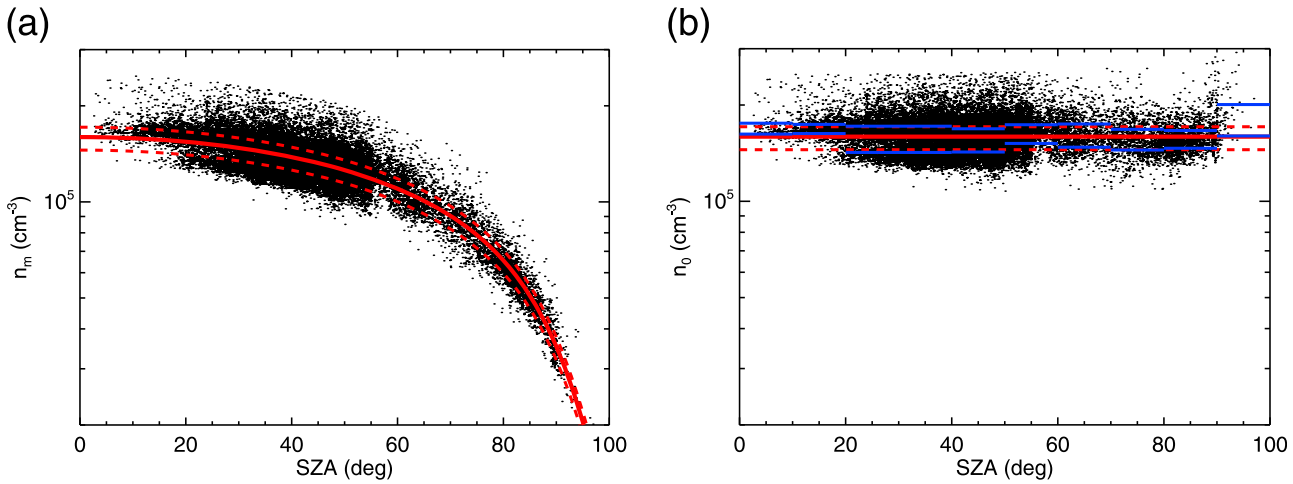

Figure 3. (a) Observed peak electron density as a function of SZA is shown by black points. The solid red curve represents the best fit according to the Chapman-based model (see text). The dashed red curves represent 0.25 and 0.75 quartiles. (b) Calculated peak electron density at the subsolar point as a function of SZA where the appropriate measurement was done. The solid red line represents the value corresponding to the best fit Chapman-based model, the dashed red lines represent 0.25 and 0.75 quartiles. The solid blue lines mark 0.25 and 0.75 quartiles determined for every 10° of SZA.

the three crucial parameters n_m, $H_m = H(z_m)$ and z_m as a function of SZA angle can be studied directly using the MARSIS data and the values determined from the best Chapman fits to the measured ionospheric profiles.

[19] Measured peak electron densities n_m as a function of SZA are shown by black points in Figure 3a. Taking into account that an increase in H with altitude causes in general the peak electron density n_m to decrease with SZA faster than $\sim 1/\sqrt{\mathrm{Ch}}$ predicted by the Chapman theory, the observed dependence can be expressed by an empirical relation:

$$n_m = \frac{n_0}{\mathrm{Ch}^k} \tag{4}$$

where $k > 0.5$ [*Hantsch and Bauer*, 1990, and references therein]. The best fit obtained using equation (4) is shown by a solid red curve in Figure 3a. The values of appropriate parameters are $k = 0.546 \pm 0.001$ and $n_0 = 1.59 \times 10^5$ cm^{-3} ± 0.1%. The values of n_0 calculated for each of the profiles are shown in Figure 3b as a function of SZA. Solid blue lines marking 0.25 and 0.75 quartiles determined for every 10° of SZA are shown in order to demonstrate that the values of n_0 do not exhibit any clear trend. The only exception might be at SZA > 90° where the observed densities seem to be larger than the predicted ones. This is consistent with results obtained by *Gurnett et al.* [2008] and can be most probably explained by additional ionization sources such as plasma transport and impact ionization by precipitating electrons that have to be taken into account beyond the terminator [*Fox and Brannon*, 1993; *Němec et al.*, 2010].

[20] We have also estimated the scatter of data points around the median value. The two dashed red lines at values 1.45×10^5 cm^{-3} and 1.71×10^5 cm^{-3} mark 0.25 and 0.75 quartiles. The corresponding 0.25 and 0.75 quartile dependencies of n_m as a function of SZA are plotted in Figure 3a by dashed red curves. The values of n_0 and k obtained are in good agreement with previously reported values. Namely, *Nielsen et al.* [2006], *Fox and Yeager* [2006], and *Morgan et al.* [2008] reported the values of $n_0 = 1.79 \times 10^5$ cm^{-3}, $n_0 = (1.82 \pm 0.03) \times 10^5$ cm^{-3} and $n_0 = 1.58 \times 10^5$ cm^{-3} ± 0.01%, respectively. *Hantsch and Bauer* [1990] reported $k = 0.57$, while *Nielsen et al.* [2006] obtained a value of $k = 0.48$ and *Fox and Yeager* [2006] obtained a value of $k = 0.465 \pm 0.010$. However, they used the equation (4) with the approximation Ch = 1/cos(SZA), resulting in a decrease of k as the terminator is approached [*Fox and Yeager*, 2006].

[21] Figure 4 uses the same representation as Figure 3, but it deals with the dependence on SZA of neutral scale height H_m at the altitude of peak electron density. Although the Chapman theory assumes no correlation between H_m and SZA, it can be seen that H_m increases with increasing SZA. This is most likely due to the fact that H_m at larger SZAs corresponds to higher altitudes. In other words, the primary reason for the effect is an altitude rather than a SZA dependence of H. The increase of H with increasing altitude is well documented by *Withers* [2006, Figure 2e] obtained using Mars Global Surveyor and Mars Odyssey accelerometer measurements and is consistent with models of the Martian ionosphere [*Krasnopolsky*, 2002, and references therein]. Taking into account the form of equation (3), it is found that the observed dependence approximately follows

$$H_m = H(z_m) = H_0 + l \ln \mathrm{Ch} \tag{5}$$

The values of the best fit parameters are $l = 3.43 \pm 0.04$ km and $H_0 = 12.16 \pm 0.03$ km. The values of 0.25 and 0.75 quartiles of the H_0 parameter are 10.02 km and 13.88 km, respectively. Solid blue lines in Figure 4b marking 0.25 and 0.75 quartiles determined for every 10° of SZA demonstrate that there is no clear trend in H_0 with the exception of SZA > 90°. The predicted values of H_m beyond the terminator are larger than the observed ones. This might be related to the peak altitude at these large SZAs being so high that it is out of the main region of neutral temperature

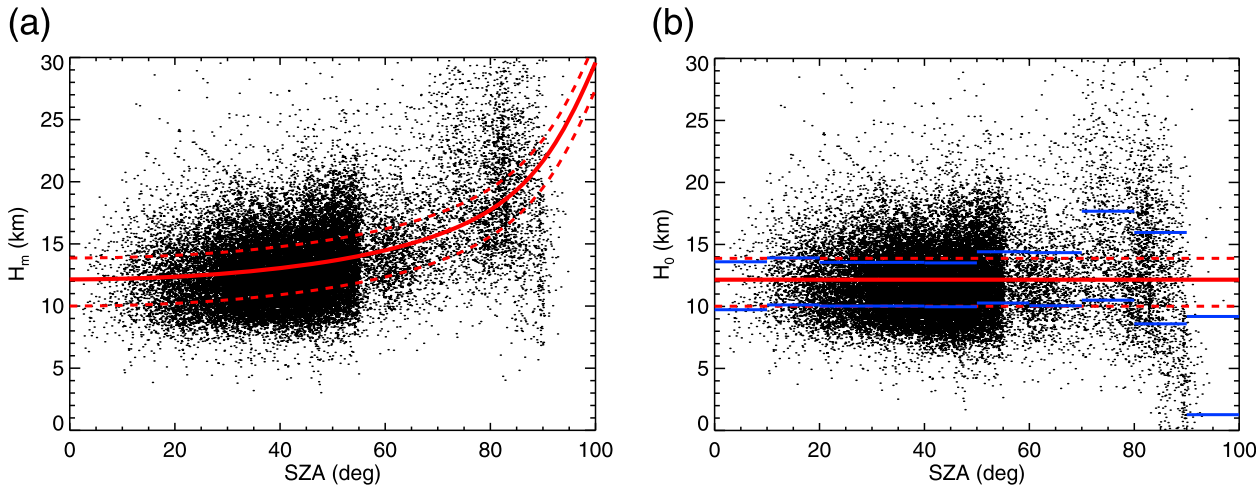

Figure 4. (a) Neutral scale height close to the altitude of peak electron density determined from the best fit Chapman model as a function of SZA. The solid red curve represents the best fit according to the used empirical model (see text). The dashed red curves represent 0.25 and 0.75 quartiles. (b) Calculated neutral scale height at the ionospheric peak at the subsolar point as a function of SZA where the appropriate measurement was done. The solid red line represents the value corresponding to the best fit empirical model; the dashed red lines represent 0.25 and 0.75 quartiles. The solid blue lines mark 0.25 and 0.75 quartiles determined for every 10° of SZA.

increase [see *Krasnopolsky* 2002, Figure 1] or it may indicate a decrease of the neutral temperature close to the terminator. The obtained values of l and H_0 correspond to $\frac{dH}{dz}(z_0) = \frac{l}{H_0} \approx 0.28$. This is larger, but at least roughly comparable with results by *Withers* [2006] and *Krasnopolsky* [2002] (approximately 0.12 and 0.06 according to *Withers* [2006, Figure 2e] and *Krasnopolsky* [2002, equation in paragraph 14] for low solar activity, respectively).

[22] Finally, the results of the same analysis for the altitude of peak electron density z_m are shown in Figure 5. Since the altitude of the ionospheric peak, unlike the peak electron density, is not very sensitive to a change of the neutral scale height above the ionospheric peak [*Wang and Nielsen*, 2004] and, moreover, equation (3) seems to express reasonably well the dependence observed in the data, no additional correction was introduced to the original Chapman theory regarding the parameter z_m. It is assumed that the dependence follows equation (3) with the value of $H = H_0$. The best fit parameter z_0 is found to be $z_0 = 124.7 \pm 0.1$ km. The parameter z_0 for the 0.25 and 0.75 quartiles is equal to 117.0 km and 132.6 km, respectively. Solid blue lines in Figure 5b marking 0.25 and 0.75 quartiles determined for every 10° of SZA demonstrate that there is no clear trend in z_0.

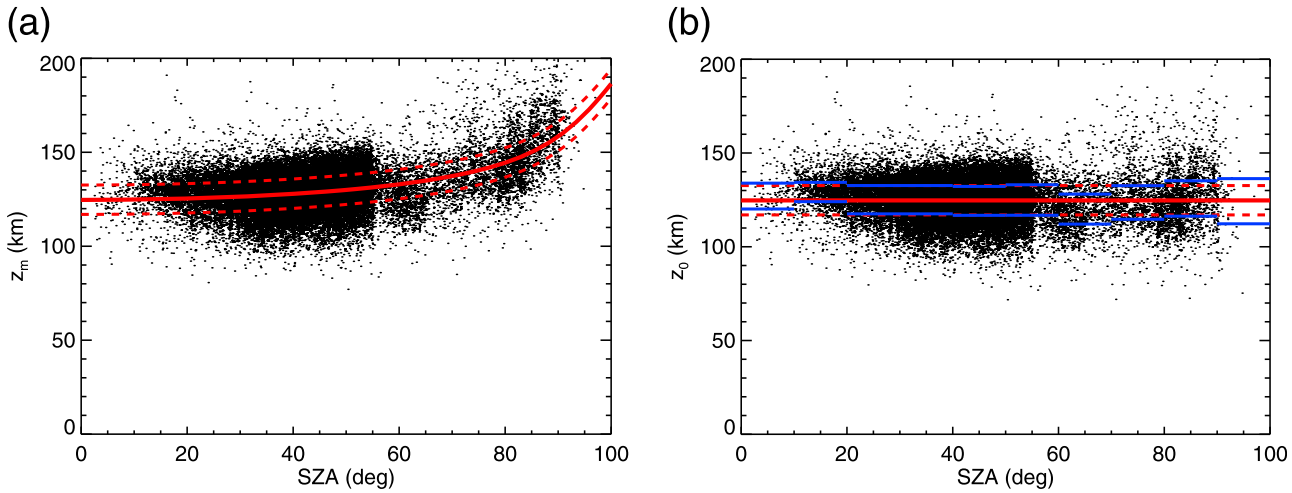

Figure 5. (a) Altitude of peak electron density as a function of SZA. The solid red curve represents the best fit according to the Chapman-based model (see text). The dashed red curves represent 0.25 and 0.75 quartiles. (b) Calculated altitude of peak electron density at the subsolar point as a function of SZA where the appropriate measurement was done. The solid red line represents the value corresponding to the best fit Chapman-based model; the dashed red lines represent 0.25 and 0.75 quartiles. The solid blue lines mark 0.25 and 0.75 quartiles determined for every 10° of SZA.

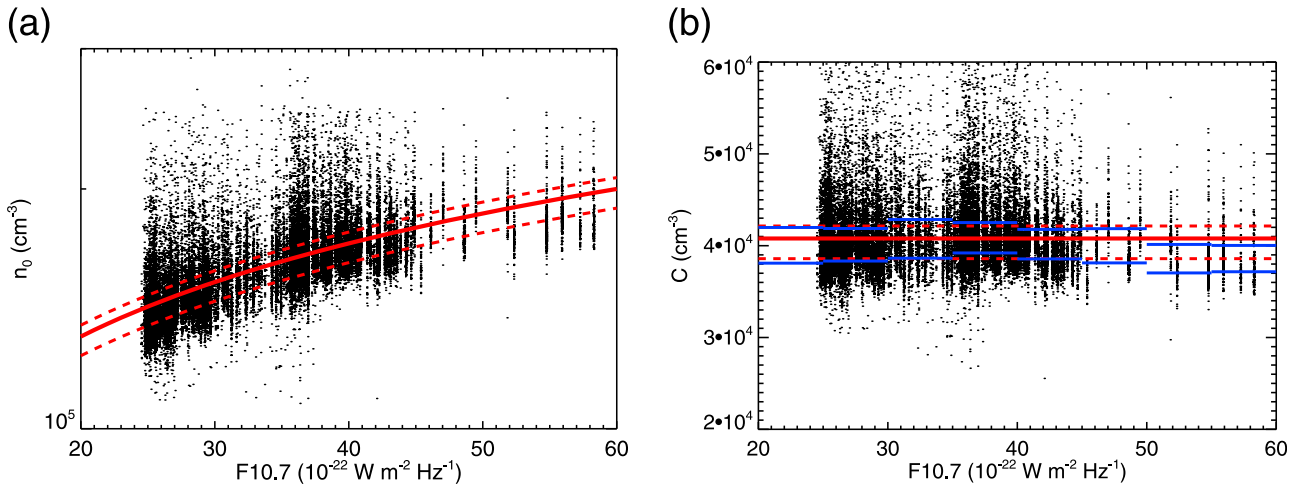

Figure 6. (a) Calculated peak electron density at the subsolar point as a function of estimated $F_{10.7}$ solar flux (see text). The solid red curve represents the best fit supposing a power law dependence. The dashed red curves represent 0.25 and 0.75 quartiles. (b) The constant from the power law dependence on $F_{10.7}$ given in equation (6) as a function of $F_{10.7}$ solar flux where the appropriate measurement was done. The solid red line represents the value corresponding to the best fit power law dependence; the dashed red lines represent 0.25 and 0.75 quartiles. The solid blue lines mark 0.25 and 0.75 quartiles determined for every 5×10^{-22} W m^{-2} Hz^{-1} of $F_{10.7}$.

[23] Except for this basic dependence of the used parameters on SZA, it is clear that the electron density in the ionosphere also depends on the intensity of the ionization source, i.e. on the incoming solar radiation. This can be approximated by solar radio flux $F_{10.7}$ [*Hantsch and Bauer*, 1990; *Morgan et al.*, 2008; *Withers*, 2009]. However, the values of $F_{10.7}$ are sampled at the Earth orbit and their recalculation to Mars is rather tricky. As discussed by *Morgan et al.* [2008], two different corrections are needed. First, it is necessary to compensate for larger (and varying) Sun distance as compared to Earth. This can be done given the known Sun-Mars distance and supposing that the solar radio flux varies inversely with the square of the distance. The need for the second correction stems from the relative orbital position of Mars and Earth, i.e. from the fact that they are in general not "aligned". Following *Morgan et al.* [2008], we use the idea that the first-order variation of $F_{10.7}$ is due to the solar rotation and we account for this by taking a weighted average of samples measured at Earth at present Mars azimuth on the solar rotation before and after the sampling time at Mars.

[24] The values of peak electron densities in the subsolar point n_0 as a function of solar radio flux $F_{10.7}$ are shown in Figure 6a. Following *Withers* [2009, and references therein] we suppose that

$$n_0 = CF_{10.7}^m \tag{6}$$

and obtain the best fit values $C = 40{,}786$ cm^{-3} ± 1% and $m = 0.388 \pm 0.003$. The resulting dependence is shown by a solid red curve. Similar to those for the previous parameters, the values of C obtained for each of the data points are shown in Figure 6b as a function of SZA. The values of 0.25 and 0.75 quartiles are equal to 38,585 cm^{-3} and 42,145 cm^{-3}, respectively. Solid blue lines in Figure 6b marking 0.25 and 0.75 quartiles determined for every 5×10^{-22} W m^{-2} Hz^{-1} of $F_{10.7}$ demonstrate that there is no clear trend in C. The only minor deviation is at large values of $F_{10.7}$, where the observed electron densities are somewhat lower than predicted. However, taking into account that the used values of $F_{10.7}$ are only estimates determined by weighted averaging (see above), it is difficult to make any firm conclusions from this. The obtained value of m is in rough agreement with the previously reported values: $m = 0.36$ [*Hantsch and Bauer*, 1990], $m = 0.37 \pm 0.06$ [*Breus et al.*, 2004], $m = 0.30 \pm 0.04$ [*Morgan et al.*, 2008].

[25] Although the estimate of solar radio flux $F_{10.7}$ at Mars includes Sun-Mars distance (see its calculation above), we have also analyzed the dependence on Sun-Mars distance separately. Values of H_0 do not exhibit any strong dependence either on solar radio flux $F_{10.7}$ or on Sun-Mars distance (the values of Spearman's correlation coefficients are about 0.08 and −0.11, respectively.) However, the values of peak altitudes z_0 at the subsolar point show a significant correlation with the Sun-Mars distance [*Morgan et al.*, 2008]: the value of Spearman's correlation coefficient is about −0.59. This can possibly be explained by cooling of the atmosphere during the periods when Sun-Mars distance is larger [*Kliore et al.*, 1973]. The values of z_0 as a function of $1/R^2$ where R is the Sun-Mars distance in AU are shown in Figure 7a. It can be seen that z_0 systematically increases with $1/R^2$, i.e. z_0 is higher when the Sun-Mars distance is lower. We have approximated this dependence by a simple linear fit:

$$z_0 = z_0^{(A)} + \frac{z_0^{(B)}}{R^2} \tag{7}$$

and obtained the best fit values $z_0^{(A)} = 83.5 \pm 0.4$ km and $z_0^{(B)} = 92.4 \pm 0.8$ km AU^2. The resulting dependence is shown by a solid red curve. The values of $z_0^{(A)}$ obtained for each of the data points are shown in Figure 7b as a function

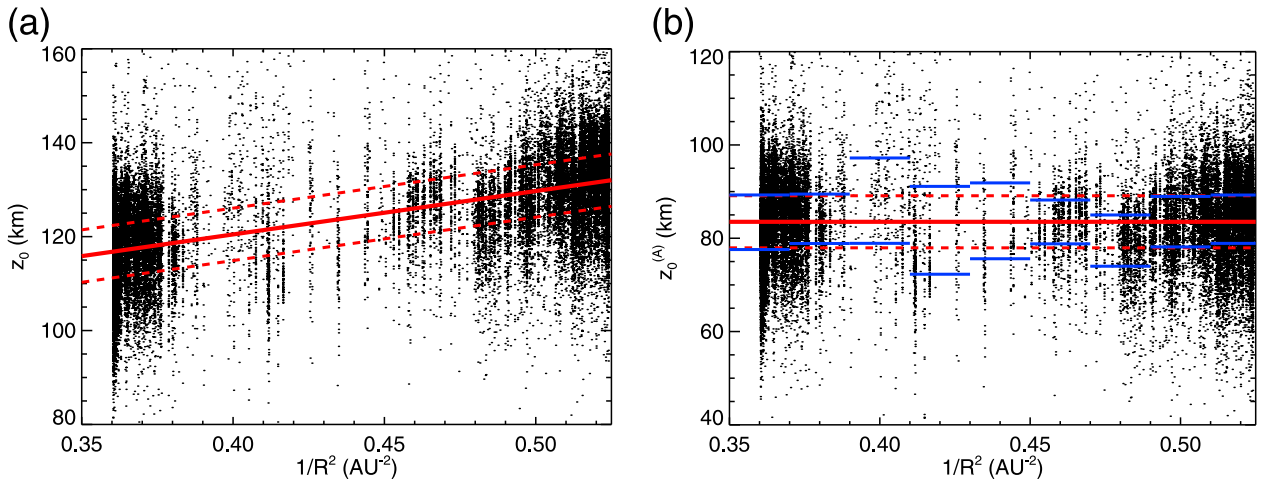

Figure 7. (a) Altitude of peak electron density at the subsolar point as a function of $1/R^2$, where R is the Sun-Mars distance in AU. The solid red curve represents the best fit supposing a linear dependence. The dashed red curves represent 0.25 and 0.75 quartiles. (b) The constant from the linear dependence given in equation (7) as a function of $1/R^2$, using the value of R where the appropriate measurement was done. The solid red line represents the value corresponding to the best fit; the dashed red lines represent 0.25 and 0.75 quartiles. The solid blue lines mark 0.25 and 0.75 quartiles determined for every 0.02 AU^{-2} of $1/R^2$.

of $1/R^2$. The values of 0.25 and 0.75 quartiles are equal to 77.9 km and 89.1 km, respectively. Solid blue lines in Figure 7b determined for every 0.02 AU^{-2} of $1/R^2$ demonstrate that there is no clear trend in $z_0^{(A)}$.

4. Diffusion Region

[26] As can be seen from Figure 2, the median electron density in the diffusion region as well as the 0.25 and 0.75 quartiles decrease exponentially with increasing altitude. However, as reported by *Duru et al.* [2008], the appropriate diffusion scale height increases significantly as a function of SZA. This effect is studied in detail in Figure 8. For each interval of SZAs, all available local electron density measurements were used to evaluate the median and the 0.25/0.75 quartile values of electron density as a function of altitude. This median/quartile profiles

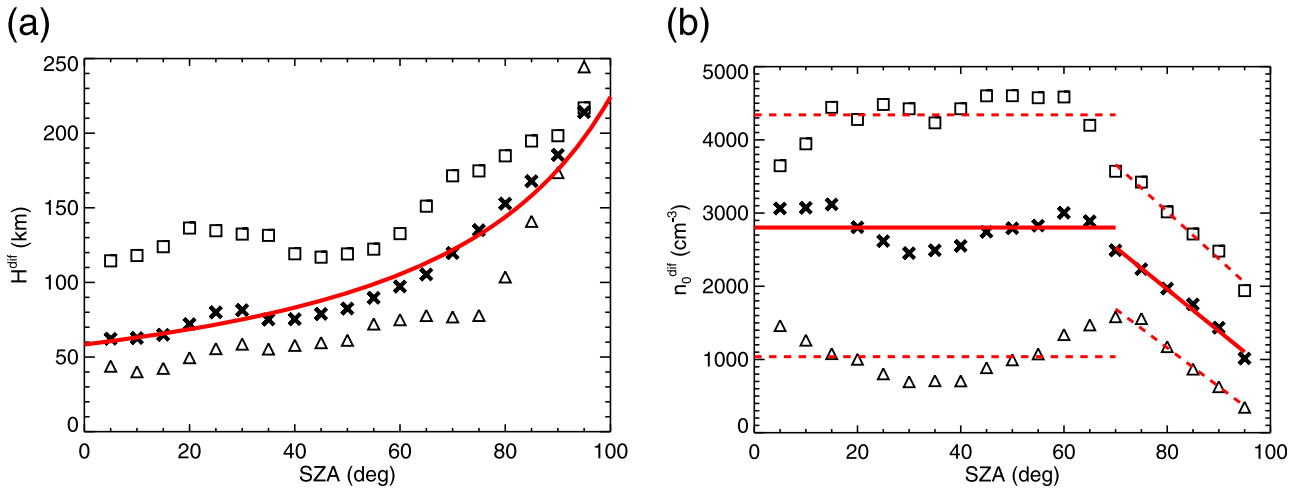

Figure 8. (a) Diffusion scale height determined from local measurements of electron density as a function of SZA. The values obtained for median profiles are shown by crosses, the values obtained for 0.25 quartile profiles are shown by triangles, and the values obtained for 0.75 quartile profiles are shown by squares. The red curve represents a fit taking into account the inclination of magnetic field induced in the ionosphere due to the interaction with solar wind (see text). (b) Electron density at the reference altitude $z_0^{dif} = 325$ km as a function of SZA. The meaning of the individual symbols is the same as in Figure 8a. The solid red horizontal line shows the mean value obtained for the median profiles at SZA < 70°. The mean values obtained for 0.25 and 0.75 quartile profiles at SZA < 70° are shown by the dashed red horizontal lines. The solid red line and the dashed red lines at SZA ≥ 70° represent a linear fit to the median and quartile profiles at large SZAs, respectively.

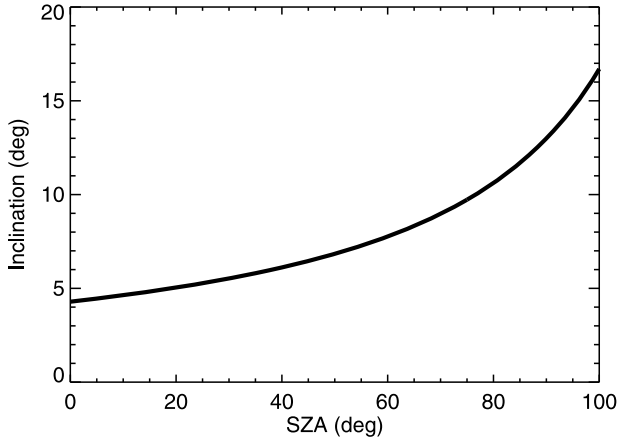

Figure 9. Inclination of the induced magnetic field determined using B_r = 3 nT and B_h from equation (9).

were then, for a given reference altitude z_0^{dif}, fitted by an exponential:

$$n = n_0^{dif} \exp\left(-\frac{z - z_0^{dif}}{H^{dif}}\right) \quad (8)$$

to determine the values n_0^{dif} and H^{dif}.

[27] The resulting values of H^{dif} and n_0^{dif} are shown as a function of SZA in Figures 8a and 8b, respectively. Each data point represents the results obtained for the 20° interval of SZA centered at the point. The values of H^{dif} and n_0^{dif} obtained for the median profiles are shown by crosses, the values obtained for the 0.25 quartile profiles are shown by triangles and the values obtained for the 0.75 quartile profiles are shown by squares. The reference altitude used was z_0^{dif} = 325 km. This value was chosen, because the electron densities at this altitude are expected not to change significantly with SZA up to about 80° [*Duru et al.*, 2008]. This is in good agreement with the dependence observed in Figure 8b. Note that the change of n_0^{dif} at SZA ≈ 70° as compared to the change of n_0^{dif} at SZA ≈ 80° reported by *Duru et al.* [2008] is due to the 20° wide bins used in the present study. This change is in good agreement with ionospheric simulation models [*Duru et al.*, 2008]. Qualitatively, it can be understood in such a way that up to SZA ≈ 80° an increase of diffusion scale height with SZA compensates for decreasing peak electron density. However, at large SZAs the decrease of peak electron density with SZA is so fast that the increase of diffusion scale height cannot compensate for it anymore. The solid red horizontal line in Figure 8b at $n_0^{dif} = 2800 \pm 120$ cm^{-3} shows the mean value of n_0^{dif} obtained for median profiles at SZA < 70°. The mean values of n_0^{dif} obtained for 0.25 and 0.75 quartile profiles are shown by dashed red horizontal lines at values of n_0^{dif} = 1040 cm^{-3} and n_0^{dif} = 4340 cm^{-3}, respectively. At larger SZAs the values of n_0^{dif} decrease systematically. The decrease of n_0^{dif} corresponding to median profiles at SZA ≥ 70° can be approximated by a linear dependence: n_0^{dif} = 6530 cm^{-3} −57 cm^{-3}/deg × SZA. The dependencies corresponding to 0.25 and 0.75 quartile profiles have about the same slope but are shifted toward lower/larger densities, respectively (see Figure 8b).

[28] The diffusion scale height H^{dif} of the median profile depicted in Figure 8a increases monotonically with SZA, ranging from about 60 km near the subsolar point to nearly 200 km close to the terminator. The diffusion scale height of the 0.25 quartile profile follows the same dependence, but it is generally somewhat lower. Similarly, the diffusion scale height of the 0.75 quartile profile is found to be in general larger than the diffusion scale height of the median profile, being in good agreement with Figure 2. The difference in the diffusion scale heights of median and quartile profiles significantly decreases at large SZAs, approaching zero near the terminator. It means that the distribution of observed electron densities does not get broader at higher altitudes. This can be probably explained by the inclination of the induced magnetic field in this region being large enough to enable a close relation between electron densities over a large range of altitudes. At lower SZAs this is prevented by nearly horizontal induced magnetic field that slows down any vertical plasma transport (see below).

[29] Taking into account that the crustal magnetic fields seem to have little influence [*Duru et al.*, 2008], the reason that H^{dif} increases with SZA can be understood in terms of the magnetic field induced in the ionosphere due to interaction with the solar wind. This magnetic field impedes vertical transport of plasma [*Shinagawa and Cravens*, 1989, 1992]. Since it is primarily horizontal at the subsolar point and its inclination slowly increases toward the terminator [*Brain et al.*, 2003; *Crider et al.*, 2004], the diffusion scale height is expected to increase with SZA. Assuming that the plasma diffusion occurs primarily along magnetic field lines, the vertical plasma scale height is in the first approximation reduced by a factor sin$I$, where I is the inclination of the magnetic field [*Rishbeth and Garriott*, 1969; *Schunk and Nagy*, 2000].

[30] The value of the magnetic field inclination I at an altitude of about 400 km as a function of SZA can be approximately estimated from *Brain et al.* [2003, Figure 7], which shows both radial and horizontal component of the induced magnetic field as a function of SZA. While the radial component of the induced magnetic field B_r remains nearly constant at about 3 nT all over the analyzed SZA range, the horizontal component of the induced magnetic field B_h decreases monotonically with increasing SZA. Although no approximate analytical formula to express this dependence was given by *Brain et al.* [2003, Figure 7], they suggest that in the SZA range of interest the horizontal component of the induced magnetic field can be roughly described by a simple linear dependence:

$$B_h = 40 \text{ nT} - 0.3 \text{ nT/deg} \times \text{SZA} \quad (9)$$

Knowing the radial and horizontal components of the induced magnetic field, its inclination I can be calculated as I = arctan (B_r/B_h). The resulting dependence of the inclination I on SZA shown in Figure 9 is in reasonably good agreement with the dependence presented by *Crider et al.* [2004, Figure 7a]. We suppose this value at any given SZA to be constant with altitude. Although this does not exactly correspond to the real situation, because the inclination I has been found to increase with altitude [*Crider et al.*, 2004], it is a sufficient approximation for a rough

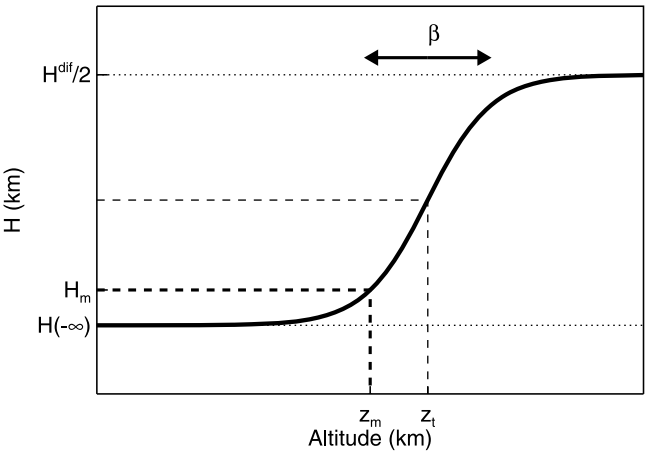

Figure 10. Empirical approximation of the scale height used in varying Chapman function as a function of altitude. Values of some key parameters used in the definition are marked.

estimate of the SZA dependence. The red curve in Figure 8a was obtained as

$$H^{dif} = H_0^{dif} \sin I \tag{10}$$

where $H_0^{dif} = 781 \pm 27$ km is a constant corresponding to the diffusion scale height in the absence of the magnetic field. It was calculated from the values $H_{dif}/\sin I$ determined separately for each of the crosses in Figure 8a.

[31] Knowing the value of the diffusion scale height H_0^{dif}, we can try to estimate the plasma temperature in the ionosphere. One has to assume the absence of upward fluxes and, moreover, that the plasma temperature does not change with altitude [*Fox and Yeager*, 2006]. Taking into account diffusive equilibrium with the electron temperature T_e of the order of twice the ion temperature T_i [*Hanson and Mantas*, 1988], $T_e = 2T_i$, the scale height should be given by $H_0^{dif} = 3kT_i/m_i g$, where m_i is the ion mass. Assuming that the diffusing ions are mainly O_2^+ [*Hanson et al.*, 1977; *Krasnopolsky*, 2002] and taking the value of $g \approx 2.82\ \mathrm{m \cdot s^{-2}}$ which corresponds to the altitudes of about 500 km above the Mars surface, one obtains $T_i \approx 2840$ K and $T_e \approx 5680$ K. This is in a rough agreement with previously reported temperatures [*Hanson et al.*, 1977; *Hanson and Mantas*, 1988].

5. Transition Between the Two Regions

[32] Having studied separately the Chapman region and the diffusion region and knowing thus the limiting dependencies at low and high altitudes, our last goal is to construct an empirical model that would describe the electron density at all altitudes. At low altitudes this model should converge to the Chapman profile given by equation (1), at high altitudes it should converge to an exponential dependence given by equation (8). At medium altitudes there should be a smooth transition between the two.

[33] Such an empirical model can be conveniently described in terms of α-Chapman functions with scale heights $H(z)$ that vary with altitude [*Rishbeth and Garriott*, 1969; *Reinisch et al.*, 2004, 2007; *Triskova et al.*, 2007]:

$$n(z) = n_m \left(\frac{H_m}{H(z)}\right)^{1/2} \exp\frac{1}{2}\{1 - y(z) - \exp[-y(z)]\} \tag{11}$$

$$y(z) = \int_{z_m}^{z} \frac{dz}{H(z)} \tag{12}$$

where n_m, z_m and H_m are the electron density, altitude, and scale height of the ionospheric peak at a given SZA. One can see that if $H(z) = H_m$ at all altitudes z, then $y(z) = \frac{z - z_m}{H_m}$ and equation (11) reduces to the ideal Chapman function given by equation (1). At high altitudes, $y(z) \gg 1$ and $y(z) \gg \exp[-y(z)]$ and equation (11) becomes an exponential decay with $y(z)$.

[34] *Reinisch et al.* [2007] suggested that an empirical function using the hyperbolic tangent can be used to describe the smooth transition between two values of scale height. We suppose the scale height to increase with altitude as:

$$H(z) = \frac{\frac{H^{dif}}{2} - H(-\infty)}{2} \tanh\left(\frac{z - z_t}{\beta}\right) + \frac{\frac{H^{dif}}{2} + H(-\infty)}{2} \tag{13}$$

where z_t, $H(-\infty)$ and β are unknown parameters. A schematic representation of the dependence expressed by equation (13) is shown in Figure 10.

[35] The values of individual parameters must be determined such that the resulting ionospheric profile fulfills two required conditions. First, the ionospheric profile at high altitudes must follow an exponential decrease with a known diffusion scale height H^{dif}. Since $lim_{z \to +\infty} \tanh(\frac{z - z_t}{\beta}) = 1$, one can see that $\lim_{z \to +\infty} H(z) = H^{dif}/2$. At high altitudes, it is thus $y(z) \approx \frac{2(z - zm)}{H^{dif}}$ and the ionospheric densities given by equation (11) follow the desired exponential dependence (8). Second, the ionospheric profile at low altitudes must follow the Chapman profile with known parameters n_m, z_m and H_m. This requirement is fulfilled by putting $H(z_m) = H_m$. Such a condition enables us to express one of the unknown parameters using the remaining ones, decreasing the number of unknown parameters to two. We have arbitrarily chosen to express the parameter $H(-\infty)$:

$$H(-\infty) = \frac{H_m - \frac{H^{dif}}{4}\left[1 + \tanh\left(\frac{z_m - z_t}{\beta}\right)\right]}{\frac{1}{2}\left(1 - \tanh\frac{z_m - z_t}{\beta}\right)} \tag{14}$$

[36] There are two remaining parameters, z_t and β. Regarding equation (13), one can see that the parameter β has the meaning of a scale length expressing the size of the transition region and as such cannot be determined from the limiting dependencies at low and high altitudes. On the other hand, for a given value of β the value of z_t is given by the condition that at high altitudes not only the correct slope of the exponential dependence has to be followed, but also the absolute values of electron densities must be correct. However, it is not simple to express the value of z_t analytically. The appropriate value must be, for a given combination of other parameters, determined numerically. The

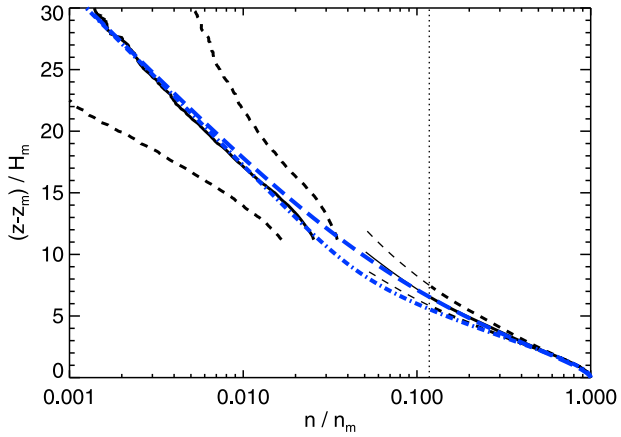

Figure 11. Same as Figure 2 but for the two extreme values of γ: the dash-dotted blue curve was obtained for $\gamma = 3$, and the dashed blue curve was obtained for $\gamma = 11$.

only free parameter in the described approach is therefore the scale length of the transition region β.

[37] The value of parameter β determines the shape of the ionospheric profile in the transition region, and vice versa, the shape of the ionospheric profile in the transition region is needed to determine the value of β. Unfortunately, there is a lack of measured data in this crucial region (see Figure 2) and therefore the value of β can be determined only approximately. Assuming that the size of the transition region is proportional to the neutral scale height, it is convenient to write $\beta = \gamma H_m$. Moreover, assuming that γ is constant over the analyzed range of SZAs, we can determine its value in such a way that it corresponds to the experimental dependence from Figure 2. Since γ corresponds roughly to the interval between the places where the data start to diverge from their respective fits, Figure 2 places some obvious constraints on the value of γ. Values of γ that are too low ($\gamma < 1$) or too high ($\gamma > 20$) are clearly unacceptable. It is found that the ionospheric profile obtained for $\gamma = 7$ expresses the observed parts of the median ionospheric profile rather well. The resulting dependence is shown in Figure 2 by a solid blue curve. It is difficult to provide any uncertainties on γ. However, γ is most certainly within the interval 3–11. The two extreme dependencies obtained for $\gamma = 3$ and $\gamma = 11$ are shown in Figure 11 by the dash-dotted blue curve and the dashed blue curve, respectively.

6. Recapitulation of the Empirical Model

[38] The purpose of this section is to briefly summarize the form of our empirical model, so that the reader who wants to use it can find all the crucial information in one place. In this section, the 0.25 and 0.75 quartiles of individual parameters are marked by "0.25" and "0.75" upper indices, respectively.

[39] At altitudes up to $\approx z_0 + 5H_m$ the electron densities are calculated following the Chapman profile: $n(z) = n_m \exp\{\frac{1}{2}[1 - \frac{z-z_m}{H_m} - \exp(-\frac{z-z_m}{H_m})]\}$. The Chapman grazing incidence function Ch can be approximated by 1/cos(SZA) for SZA < 75°. The values of individual parameters are determined as follows:

[40] 1. $z_m = z_0 + H_0$ lnCh, where $H_0 = 12.16 \pm 0.03$ km, $H_0^{0.25} = 10.02$ km and $H_0^{0.75} = 13.88$ km. The value of z_0 can be taken either as $z_0 = 124.7 \pm 0.1$ km, $z_0^{0.25} = 117.0$ km, $z_0^{0.75} = 132.6$ km or, better, calculated for a given Sun-Mars distance R as: $z_0 = z_0^{(A)} + z_0^{(B)}/R^2$, where $z_0^{(A)} = 83.5 \pm 0.4$ km, $z_0^{(A)0.25} = 77.9$ km, $z_0^{(A)0.75} = 89.1$ km and $z_0^{(B)} = 92.4 \pm 0.8$ km AU^2.

[41] 2. $H_m = H_0 + l$ lnCh, where $l = 3.43 \pm 0.04$ km.

[42] 3. $n_m = n_0$ Ch^{-k}, where $k = 0.546 \pm 0.001$ and n_0 can be taken either as $n_0 = 1.59 \times 10^5$ cm$^{-3} \pm 0.1\%$, $n_0^{0.25} = 1.45 \times 10^5$ cm^{-3}, $n_0^{0.75} = 1.71 \times 10^5$ cm^{-3} or, better, calculated for a given solar radio flux $F_{10.7}$ as: $n_0 = CF_{10.7}^m$, where $m = 0.388 \pm 0.003$, $C = 40{,}786$ cm$^{-3} \pm 1\%$, $C^{0.25} = 38{,}585$ cm^{-3} and $C^{0.75} = 42{,}145$ cm^{-3}.

[43] In the diffusion region, i.e. at altitudes higher than $\approx z_0 + 10H_m$, the electron densities are calculated as: $n = n_0^{dif} \exp(-(z - z_0^{dif})/H^{dif})$. The values of individual parameters are $z_0^{dif} = 325$ km, $n_0^{dif} = 2800 \pm 120$ cm^{-3}, $n_0^{dif0.25} = 1040$ cm^{-3}, $n_0^{dif0.75} = 4340$ cm^{-3}. The diffusion scale high H^{dif} is calculated as: $H^{dif} = H_0^{dif} \sin I$, where $H_0^{dif} = 781 \pm 27$ km and I is the inclination of the induced magnetic field. The value of I can be estimated as: $I = \arctan(B_r/B_h)$, where $B_r = 3$ nT and $B_h = 40$ nT − 0.3 nT/deg × SZA. The approximation of constant n_0^{dif} value is applicable for SZAs up to 70°. At larger SZAs the value of n_0^{dif} decreases with increasing SZA approximately as: $n_0^{dif} = 6530$ cm^{-3} −57 cm^{-3}/deg × SZA.

[44] At the transition altitudes between the Chapman region and the diffusion region, i.e. at altitudes between $\approx z_0 + 5H_m$ and $\approx z_0 + 10H_m$, a general empirical formula of $n(z)$ given by equations (11) and (12) must be used. The value of $H(z)$ is given by equation (13), where $\beta \approx 7H_m$, $H(-\infty)$ is given by equation (14) and z_t must be determined numerically from the condition that at high altitudes the values of electron densities follow the dependence from the previous paragraph.

7. Discussion

[45] Two different data sets acquired by the MARSIS instrument have been combined in the present study in order to obtain the best possible data coverage. The low-altitude high-density Chapman region is well covered by the data obtained from ionospheric sounding. However, at higher altitudes the densities are too low to be measured by this method and local measurements of electron plasma frequency have been used to determine the electron density. Unfortunately, since these are local measurements, they are limited only to altitudes higher than the periapsis altitude, which is about 300 km. Consequently, there is a significant range of altitudes from about 200–250 km to about 300 km which is not sufficiently covered by the measurements.

[46] Another complication stems from the fact that there is no strict detection threshold of the ionospheric sounding; although it is usually about 10^4 cm^{-3}, it may significantly vary from case to case. Calculating the median and 0.25 and 0.75 quartile profiles directly from the ionospheric sounding data is therefore in principle possible only for electron densities larger than the maximum detection threshold of all the events. At lower densities low-density profiles cannot be measured properly and only high-density profiles are included in the analysis, which results in overestimating the median/quartile values. We have at least partially solved this problem by using an exponential interpolation between the lowest-density ionospheric sounding data point and the data point

obtained from the local measurement. These interpolated values were then included in the analysis and used for calculating the median/quartile values. Although this approach significantly expands the density range where reasonable results can be obtained, the obtained values of electron density are a bit overestimated. This is due to the fact that the exponential interpolation assumes a constant scale height, while in the real situation the scale height increases with altitude. This overestimating effect can be seen in Figure 2, where the median/quartile values in the Chapman and diffusion regions do not connect very well. Because of this effect, the median/quartile electron densities determined from the ionospheric sounding (and exponential interpolation, if needed) should not be trusted at densities lower than the median detection threshold marked by a vertical dotted line in Figure 2. It can be seen in Figure 2 that our empirical model actually compensates for this overestimate: the model fit is noticeably to the left of the median data line at densities lower than the median detection threshold.

[47] The approach of fitting a Chapman profile to each electron density profile obtained from ionospheric sounding enabled us to obtain for each of them the three Chapman parameters n_m, z_m and H_m. These parameters were used in the further analysis, enabling us to study subtler effects than the approach used by *Morgan et al.* [2008], who analyzed directly the measured electron densities as a function of SZA. We have shown that the variation of the dayside ionosphere at altitudes at and slightly above the altitude of peak electron density can be well described by the Chapman theory. The observed small departures from this theory can most probably be explained in terms of the scale height parameter H increasing with altitude rather than being constant. There are two main factors that can cause the increase of H with altitude, probably acting simultaneously: (1) the increase of the (neutral) temperature and (2) the change of the atmospheric composition toward the lighter elements. Additionally, the electron temperature T_e increases with altitude [*Hanson and Mantas*, 1988]. This slows down the recombination rates [*Schunk and Nagy*, 2000], causing the electron densities to be larger than they would be if T_e were constant and effectively increasing the "apparent" value of H. The empirical dependencies we have found enable us to determine the Chapman parameters n_m, z_m and H_m as a function of SZA (and, optionally, of the $F_{10.7}$ solar flux and Sun-Mars distance), serving thus as a simple empirical model of the dayside ionosphere at altitudes at and slightly above the ionospheric peak.

[48] The Chapman theory is based on the assumption of a local equilibrium between the ionization and recombination at all altitudes, assuming no vertical plasma transport. However, at higher altitudes the transport processes become more important than photoionization, and eventually transport controls the structure of the dayside ionosphere [*Withers*, 2009]. This transition is well documented in the high-altitude part of Figure 2 where an exponential decrease of electron density with altitude is observed, corresponding to the situation of plasma equilibrium. Given the exponential decrease of electron density with altitude, this region of the ionosphere is conveniently described by the diffusion scale height H^{dif} and the electron density n_0^{dif} at a chosen reference altitude z_0^{dif}. Following the results of *Duru et al.* [2008], we have chosen such a reference altitude z_0^{dif} that the electron densities n_0^{dif} are nearly constant up to SZA about 70°, where they start to decrease with increasing SZA. At SZA > 70°, this would lead to model electron densities at high altitudes being larger than the real ones. In order to prevent this, a value of n_0^{dif} determined using a linear fit should be used at large SZAs (see section 4 and Figure 8b).

[49] Moreover, our results confirm that the diffusion scale height H^{dif} increases with increasing SZA, as reported by *Duru et al.* [2008]. *Duru et al.* [2008] suggested that this could be interpreted in terms of the temperature increasing with SZA, varying between about 285 and 520 K on the dayside. These temperature estimates are significantly below the previously reported values [*Hanson et al.*, 1977; *Hanson and Mantas*, 1988] and, moreover, there is no clear reason why the temperature should increase with SZA. The explanation that we propose is based on the diffusion being affected by the magnetic field induced in the ionosphere due to the interaction with the solar wind [*Shinagawa and Cravens*, 1989, 1992]. Since this magnetic field is primarily horizontal, it effectively slows down diffusion, i.e., it decreases the diffusion scale height. Taking into account the increase in inclination of the induced magnetic field with SZA [*Brain et al.*, 2003; *Crider et al.*, 2004], this explanation seems to be in agreement with the observed dependence of the diffusion scale height (see the red curve in Figure 8a). Finally, the resulting temperature estimates of $T_i \approx 2840$ K and $T_e \approx 5680$ K correspond reasonably well with the previously reported values; according to *Hanson et al.* [1977, Figure 7] the ion temperature at altitudes close to 300 km should be about 2000 K and T_e is of the order of twice the ion temperature [*Hanson and Mantas*, 1988]. Note that our values of T_i and T_e are expected to be slightly larger than the values reported by *Hanson et al.* [1977]; *Hanson and Mantas* [1988], because they were obtained for higher altitudes.

[50] Concerning the possible influence of the crustal magnetic fields, these do not seem to significantly affect the results obtained. As argued by *Duru et al.* [2008], this might be partly because the sample interval covers periods with variations due to seasonal changes, heliocentric distance of Mars, solar activity, solar wind pressure, etc., averaging out any minor control due to the crustal magnetic field. Moreover, the magnitude of crustal magnetic field decreases with increasing altitude and at an altitude of 400 km its median value is according to *Cain et al.* [2003] model only about 5 nT. This is a rather small value as compared to the magnitude of the magnetic field induced due to the interaction with solar wind, which is typically on the order of a few tens of nT. This suggests that it is the induced magnetic field rather than the crustal magnetic field that is principally responsible for retarding diffusion.

[51] Having studied the dependence of electron density on altitude both inside the low-altitude Chapman region and the high-altitude diffusion region, it is of a great interest to find an expression that would enable us to smoothly connect the two. We managed to do this using the concept of α-Chapman functions with scale heights $H(z)$ that vary with altitude. Taking into account the required behavior at low and high altitudes, all the parameters of the chosen empirical function can be determined except one, the scale length of the transition region β. We did not express the value of β absolutely in km, but rather in units of the Chapman scale height parameter

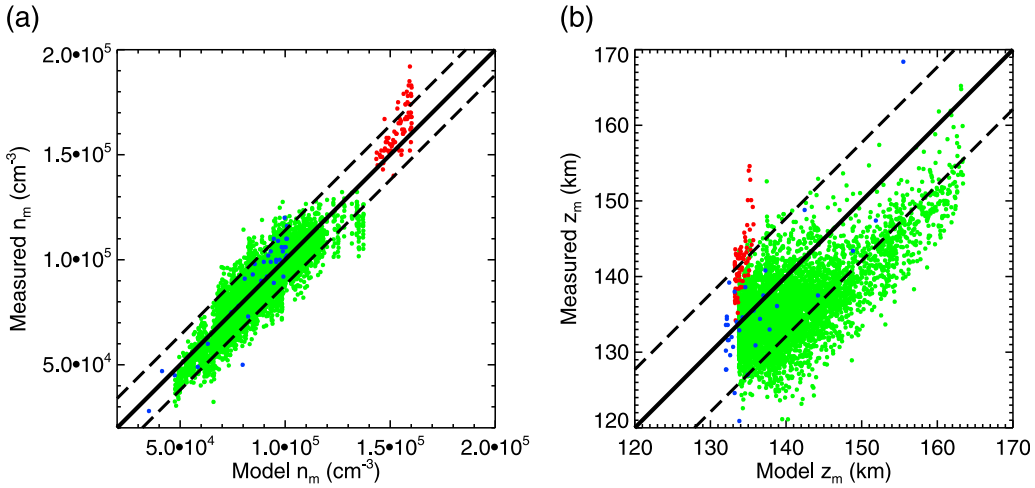

Figure 12. (a) Peak electron densities from *Kliore et al.* [1972] (red points), *Kliore et al.* [1973] (blue points), and 5600 MGS RS profiles (green points) versus model peak electron densities. The solid black line shows the 1:1 dependence. Black dashed lines correspond to 0.25 and 0.75 quartile dependencies of the model. (b) The same as Figure 12a but for peak altitudes.

H_m. Taking into account that H_m is a natural estimate of the scale height of ionospheric changes, such a normalization is rather reasonable. Moreover, it enables us to determine the value of β from the overall results displayed in Figure 2. It is in principle possible to determine the value of β in such a way that the resulting profile represents the best fit to the observed median electron profile. Unfortunately, due to the technical limitations of the MARSIS instrument there is a lack of data in this crucial region. Consequently, it was possible to determine the value of β only approximately.

[52] Concerning the accuracy of the presented empirical model, we have determined the standard deviations of individual fit parameters, along with the scatter in the data around the median dependence, expressed as quartiles. If a dependence is a function of two different parameters, we provide quartile results only for one parameter, i.e. only for the parameter that expresses the absolute value of the dependence. The other parameter describes the shape of the dependence and its uncertainty is given by the standard deviation.

[53] In order to enable a better estimate of how reliable our empirical model is, we have validated the model against other data sets. Namely, we have used the peak electron densities and altitudes published by *Kliore et al.* [1972, 1973] and 5600 MGS RS profiles available at NASA Planetary Data System [*Hinson*, 2008]. The results of this validation are presented in Figures 12 and 13 It should be mentioned that all the MARSIS data used for the construction of the model were measured during solar minimum. Median and mean Sun-Mars distance for the data included in the model were about 1.44 AU and 1.51 AU. The data of *Kliore et al.* [1972, 1973] were both measured during the solar mean, but they differed from each other by Sun-Mars distance. While the data of *Kliore et al.* [1972] were obtained for Sun-Mars distance about 1.43 AU, the data of *Kliore et al.* [1973] were obtained for Sun-Mars distance about 1.64 AU. Median Sun-Mars distance for the 5600 MGS RS profiles was about 1.56 AU, mean Sun-Mars distance was about the same. The MGS RS profiles were obtained during 1998–2005 and included data from the solar maximum.

[54] Figure 12a shows a comparison between the observed and predicted peak electron densities for the data set of *Kliore et al.* [1972] by red points, for the data set of *Kliore et al.* [1973] by blue points and for the data set consisting of 5600 MGS RS profiles by green points. It can be seen that the peak electron densities of all the data sets are in good agreement with the model. Most of the data points lie within the dashed lines that mark the 0.25 and 0.75 quartiles of the model. Figure 12b uses the same representation as Figure 12a, but it presents the results obtained for the peak altitude. The agreement between the model and the comparative data sets is slightly worse in this case. Most importantly, the peak altitudes of the MGS RS profiles seem to be somewhat lower

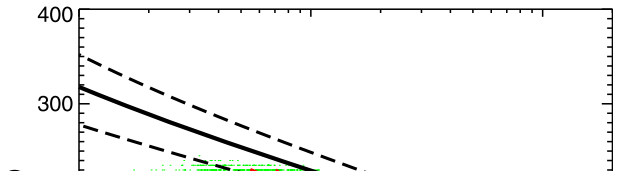

Figure 13. Electron density data from MGS RS profiles at SZAs 70°–75° resampled to the altitudinal step of 5 km are shown by green dots. Median profile and 0.25 and 0.75 quartile profiles are shown in red. Results of the empirical model obtained for the corresponding value of SZA, Sun-Mars distance and $F_{10.7}$ solar flux (see text) are shown in black. The solid black curve represents the median profile; 0.25 and 0.75 quartile profiles are shown by dashed black curves.

than predicted. However, taking into account different phases of solar cycle during the accumulation of the data, we can still say that our empirical model performs well.

[55] Finally, we have compared the predicted profile shape with the shape of the MGS RS profiles. We have chosen the interval of SZAs 70°–75°, which contains 2241 profiles out of the total 5600 MGS RS profiles. Electron densities corresponding to these profiles, resampled to the altitudinal step of 5 km are plotted in Figure 13 by green points. Median MGS RS profile in this SZA range is plotted by a solid red curve and the corresponding 0.25 and 0.75 quartile profiles are shown by dashed red curves. Results of the empirical model are shown in black. We used the parameters equal to median values of the 2241 MGS RS profiles, i.e. SZA = 73.2°, Sun-Mars distance R = 1.54 AU and $F_{10.7} = 51.7 \times 10^{-22}$ W m^{-2} Hz^{-1}.

[56] The model profile and MGS RS profiles are in reasonably good agreement. The model profile seem to slightly overestimate the electron densities. Since we have only low altitude "Chapman" portion of the profile, this is due to badly chosen values of n_m, z_m and H_m parameters. While the peak electron density is about correct, the model peak altitude is slightly higher than the peak altitude of MGS RS profiles (see above). Moreover, the model value of H_m is a bit too large. Since the MGS RS profiles were obtained at Sun-Mars distances larger than the Sun-Mars distances of the MARSIS data used for the construction of the model, this is probably at least partially related to the fact that when constructing the model we have neglected the weak negative correlation between Sun-Mars distance and H_0. However, taking into account that our model is a general empirical model designed for a large range of SZAs, Sun-Mars distances and $F_{10.7}$ values, it performs reasonably well.

8. Conclusions

[57] Dayside ionospheric profiles and local electron density measurements obtained by the MARSIS instrument were combined to provide the best electron density data coverage possible. The data were analyzed as a function of SZA, altitude, $F_{10.7}$ solar flux and Sun-Mars distance to reveal the principal dependencies governing the dayside ionosphere.

[58] We have demonstrated that there are two different regions of the dayside ionosphere with substantially different characteristics and physical mechanisms taking place. The region at altitudes up to about 5 neutral scale heights above the altitude of peak electron density is controlled primarily by photoionization and can be described by the Chapman theory. At altitudes higher than about 10 neutral scale heights above the altitude of peak electron density, the ionosphere is controlled primarily by diffusion, and the observed electron densities decrease exponentially with increasing altitude. The appropriate diffusion scale height increases with increasing SZA. This is most probably caused by the magnetic field induced in the ionosphere due to the interaction with the solar wind.

[59] Simple relations describing the electron densities in the two regions have been found. Moreover, it has been shown that it is possible to smoothly connect the photoionization and diffusion regions and to construct an empirical model of electron densities in the dayside ionosphere at altitudes above the ionospheric peak.

[60] **Acknowledgments.** The research at the University of Iowa was supported by NASA through contract 1224107 from the Jet Propulsion Laboratory.

References

Brain, D. A., F. Bagenal, M. H. Acuña, and J. E. P. Connerney (2003), Martian magnetic morphology: Contributions from the solar wind and crust, *J. Geophys. Res.*, *108*(A12), 1424, doi:10.1029/2002JA009482.

Breus, T. K., A. M. Krymskii, D. H. Crider, N. F. Ness, D. Hinson, and K. K. Barashyan (2004), Effect of the solar radiation in the topside atmosphere/ionosphere of Mars: Mars Global Surveyor observations, *J. Geophys. Res.*, *109*, A09310, doi:10.1029/2004JA010431.

Cain, J. C., B. B. Ferguson, and D. Mozzoni (2003), An n = 90 internal potential function of the Martian crustal magnetic field, *J. Geophys. Res.*, *108*(E2), 5008, doi:10.1029/2000JE001487.

Chapman, S. (1931a), The absorption and dissociative or ionizing effect of monochromatic radiation in an atmosphere on a rotating Earth, *Proc. Phys. Soc.*, *43*, 26–45.

Chapman, S. (1931b), The absorption and dissociative or ionizing effect of monochromatic radiation in an atmosphere on a rotating Earth, Part II. Grazing incidence, *Proc. Phys. Soc.*, *43*, 483–501.

Chen, R. H., T. E. Cravens, and A. F. Nagy (1978), The Martian ionosphere in light of the Viking observations, *J. Geophys. Res.*, *83*(A8), 3871–3876.

Chicarro, A., P. Martin, and R. Trautner (2004), The Mars Express mission: An overview, in *Mars Express: The Scientific Payload*, edited by A. Wilson and A. Chicarro, *ESA Spec. Publ., SP-1240*, 3–13.

Crider, D. H., et al. (2001), Magnetic field draping around Mars: Mars Global Surveyor results, *Adv. Space Res.*, *27*(11), 1831–1836.

Crider, D. H., D. A. Brain, M. H. Acuña, D. Vignes, C. Mazelle, and C. Bertucci (2004), Mars Global Surveyor observations of solar wind magnetic field draping around Mars, *Space Sci. Rev.*, *111*, 203–221.

Duru, F., D. A. Gurnett, D. D. Morgan, R. Modolo, A. F. Nagy, and D. Najib (2008), Electron densities in the upper ionosphere of Mars from the excitation of electron plasma oscillations, *J. Geophys. Res.*, *113*, A07302, doi:10.1029/2008JA013073.

Fox, J. L., and J. F. Brannon (1993), Upper limits to the nightside ionosphere of Mars, *Geophys. Res. Lett.*, *20*(13), 1391–1394.

Fox, J. L., and A. Dalgarno (1979), Ionization, luminosity, and heating of the upper atmosphere of Mars, *J. Geophys. Res.*, *84*(A12), 7315–7333.

Fox, J. L., and K. E. Yeager (2006), Morphology of the near-terminator Martian ionosphere: A comparison of models and data, *J. Geophys. Res.*, *111*, A10309, doi:10.1029/2006JA011697.

Gurnett, D. A., et al. (2005), Radar soundings of the ionosphere of Mars, *Science*, *310*, 1929–1933.

Gurnett, D. A., et al. (2008), An overview of radar soundings of the Martian ionosphere from the Mars Express spacecraft, *Adv. Space Res.*, *41*, 1335–1346.

Hanson, W. B., and G. P. Mantas (1988), Viking electron temperature measurements: Evidence for a magnetic field in the Martian ionosphere, *J. Geophys. Res.*, *93*(A7), 7538–7544.

Hanson, W. B., S. Sanatani, and D. R. Zuccaro (1977), The Martian ionosphere as observed by the Viking retarding potential analyzers, *J. Geophys. Res.*, *82*(28), 4351–4363.

Hantsch, M. H., and S. J. Bauer (1990), Solar control of the Mars ionosphere, *Planet. Space Sci.*, *38*(4), 539–542.

Hinson, D. P. (2008), Mars Global Surveyor radio occultation profiles of the ionosphere—Reorganized, *Rep. MGS-M-RSS-5-EDS-V*1.0, NASA Planet. Data Syst., Greenbelt, Md.

Jordan, R., et al. (2009), The Mars Express MARSIS sounder instrument, *Planet. Space Sci.*, *57*, 1975–1986, doi:10.1016/j.pss.2009.09.016.

Kliore, A. J., D. L. Cain, G. Fjeldbo, B. L. Seidel, M. J. Sykes, and S. I. Rasool (1972), The atmosphere of Mars from Mariner 9 radio occultation measurements, *Icarus*, *17*, 484–516.

Kliore, A. J., G. Fjeldbo, B. L. Seidel, M. J. Sykes, and P. M. Woiceshyn (1973), S Band radio occultation measurements of the atmosphere and topography of Mars with Mariner 9: Extended mission coverage of polar and intermediate latitudes, *J. Geophys. Res.*, *78*(20), 4331–4351.

Krasnopolsky, V. A. (2002), Mars' upper atmosphere and ionosphere at low, medium and high solar activities: Implications for evolution of water, *J. Geophys. Res.*, *107*(E12), 5128, doi:10.1029/2001JE001809.

Lillis, R. J., M. O. Fillingim, L. M. Peticolas, D. A. Brain, R. P. Lin, and S. W. Bougher (2009), Nightside ionosphere of Mars: Modeling the

effects of crustal magnetic fields and electron pitch angle distributions on electron impact ionization, *J. Geophys. Res.*, *114*, E11009, doi:10.1029/2009JE003379.

Morgan, D. D., D. A. Gurnett, D. L. Kirchner, J. L. Fox, E. Nielsen, and J. J. Plaut (2008), Variation of the Martian ionospheric electron density from Mars Express radar soundings, *J. Geophys. Res.*, *113*, A09303, doi:10.1029/2008JA013313.

Němec, F., D. D. Morgan, D. A. Gurnett, and F. Duru (2010), Nightside ionosphere of Mars: Radar soundings by the Mars Express spacecraft, *J. Geophys. Res.*, *115*, E12009, doi:10.1029/2010JE003663.

Nielsen, E., et al. (2006), Observations of vertical reflections from the topside Martian ionosphere, *Space Sci. Rev.*, *126*, 373–388, doi:10.1007/s11214-006-9113-y.

Picardi, G., et al. (2004), MARSIS: Mars advanced radar for subsurface and ionosphere sounding, in *Mars Express: the Scientific Payload*, edited by A. Wilson and A. Chicarro, *ESA Spec. Publ., SP-1240*, 51–69.

Reinisch, B. W., X.-Q. Huang, A. Belehaki, J.-K. Shi, M.-L. Zhang, and R. Ilma (2004), Modelling the IRI topside profile using scale heights from ground-based ionosonde measurements, *Adv. Space Res.*, *34*, 2026–2031, doi:10.1016/j.asr.2004.06.012.

Reinisch, B. W., P. Nsumei, X. Huang, and D. K. Bilitza (2007), Modelling the F2 topside and plasmasphere for IRI using IMAGE/RPI and ISIS data, *Adv. Space Res.*, *39*, 731–738, doi:10.1016/j.asr.2006.05.032.

Rishbeth, H., and O. K. Garriott (1969), *Introduction to Ionospheric Physics*, Academic, New York.

Rohrbaugh, R. P., J. S. Nisbet, E. Bleuler, and J. R. Herman (1979), The effect of energetically produced O_2^+ on the ion temeperatures of the Martian thermosphere, *J. Geophys. Res.*, *84*(A7), 3327–3338.

Schunk, R. W., and A. F. Nagy (2000), *Ionospheres: Physics, Plasma Physics, and Chemistry*, Cambridge University Press, New York.

Shinagawa, H., and T. E. Cravens (1989), A one-dimensional multispecies magnetohydrodynamic model of the dayside ionosphere of Mars, *J. Geophys. Res.*, *94*(A6), 6506–6516.

Shinagawa, H., and T. E. Cravens (1992), The ionospheric effects of a weak intristic magnetic field at Mars, *J. Geophys. Res.*, *97*(E1), 1027–1035.

Smith, F. L., and C. Smith (1972), Numerical evaluation of Chapman's grazing incidence integral ch (X,χ), *J. Geophys. Res.*, *77*(19), 3592–3597.

Triskova, L., I. Galkin, V. Truhlik, and B. W. Reinisch (2007), Application of seamless vertical profiles for use in the topside electron density modeling, *Adv. Space Res.*, *39*, 774–778, doi:10.1016/j.asr.2006.09.033.

Wang, J. S., and E. Nielsen (2004), Solar wind modulation of the Martian ionosphere observed by Mars Global Surveyor, *Ann. Geophys.*, *22*, 2277–2281.

Withers, P. (2006), Mars Global Surveyor and Mars Odyssey Accelerometer observations of the Martian upper atmosphere during aerobraking, *Geophys. Res. Lett.*, *33*, L02201, doi:10.1029/2005GL024447.

Withers, P. (2009), A review of observed variability in the dayside ionosphere of Mars, *Adv. Space Res.*, *44*, 277–307.

F. Duru, D. A. Gurnett, and D. D. Morgan, Department of Physics and Astronomy, University of Iowa, Iowa City, IA 52242, USA.

F. Němec and V. Truhlík, Institute of Atmospheric Physics, Academy of Sciences of the Czech Republic, Bocni II 1401, Prague 14131, Czech Republic. (frantisek.nemec@gmail.com)